A Stochastic Approach to Modeling Drainage Basin Evolution

Gregory E. Tucker[1] and Rafael L. Bras

Department of Civil and Environmental Engineering
Massachusetts Institute of Technology
Cambridge, MA 02139

Part I-D of final technical report submitted to U.S. Army Corps of Engineers
Construction Engineering Research Laboratory (USACERL)
by Gregory E. Tucker, Nicole M. Gasparini, Rafael L. Bras, and Stephen T. Lancaster
in fulfillment of contract number DACA88-95-C-0017

April, 1999

1. To whom correspondence should be addressed: Dept. of Civil & Environmental Engineering, MIT Room 48-429, Cambridge, MA 02139, ph. (617) 252-1607, fax (617) 253-7475, email gtucker@mit.edu

A Stochastic Approach to Modeling Drainage Basin Evolution

Although it is often modeled as a continuum process, landscape evolution is in fact driven by discrete events. The topography of a typical mountain range, for example, is shaped by a quasi-random sequence of floods, earthquakes, and landslides, with each process having its own characteristic frequency distribution, and with each frequency distribution typically varying in time and space as well. The importance of the frequency spectra of geomorphic events is a fundamental problem in geomorphic research. Much of the previous research on this problem has focussed on defining the recurrence interval of the most effective geomorphic event, with "effectiveness" defined either on the basis of denudation rate (e.g., Wolman and Miller, 1960; Andrews, 1980; Webb and Walling, 1982; Ashmore and Day, 1988) or landform genesis (e.g., Baker, 1977; Harvey, 1977; Wolman and Gerson, 1978). Scant attention has been paid, however, to the question of how variability in geomorphic forces impacts the morphology and rate of evolution of landforms. For example, the relative geomorphic significance of climate variability as opposed to mean climate has been widely debated and is not well understood. In this report, we address the problem of rainfall variability and its impact on catchment geomorphology. We do so by developing a stochastic theory for erosion and sedimentation in a drainage basin, and exploring the consequences of that theory in the framework of the CHILD model. The stochastic model is based on the rainfall model of Eagleson (1978) and describes the probability distribution of storm depth, duration, and frequency. Combining the stochastic rainfall model with the landscape evolution model enables us to simulate the long-term geomorphic impact of natural variability in storm size. We focus in particular on three questions:

1. What is the predicted sensitivity of long-term average sediment transport rates to the degree of

variability in rainfall intensity?

2. To what degree does the importance of variability depend on the presence of thresholds in the landscape, such as a threshold for sediment entrainment?
3. What are the morphologic consequences of rainfall variability?

Model Description

Stochastic Rainfall Model

Rainfall is modeled as a series of discrete random storm events, using the model of Eagleson (1978). Each storm event is treated as having a constant rainfall rate P that lasts for a duration T_r and is separated from the next event by an interstorm interval T_b. The probability density functions for storm intensity, duration, and interstorm interval are given by

Rainfall (runoff) intensity $$f(P) = \frac{1}{\bar{P}}\exp\left(-\frac{P}{\bar{P}}\right) \quad (1)$$

Storm duration $$f(T_r) = \frac{1}{\bar{T}_r}\exp\left(-\frac{T_r}{\bar{T}_r}\right) \quad (2)$$

Interstorm period $$f(T_b) = \frac{1}{\bar{T}_b}\exp\left(-\frac{T_b}{\bar{T}_b}\right) \quad (3)$$

In order to derive a distribution of runoff rates *f(R)*, we start by assuming runoff is Hortonian and uniform across the landscape. (However, the formulation could be modified to account for saturation-excess runoff production [Dunne, 1978]). Runoff rate, *R*, is defined as precipitation minus losses to infiltration, evaporation, and/or canopy and surface interception:

$$R = P - I, \qquad I = I_c + I_l, \quad (4)$$

where I_c = infiltration capacity and I_l = evaporation and interception losses. The derived distribution for R is obtained from

$$f(R) = f(P)\frac{dP}{dR}, \tag{5}$$

$$f(R) = \begin{cases} 1/\bar{P}\exp\left(-\frac{(R+I)}{\bar{P}}\right), R>0; \\ 0 \text{ otherwise.} \end{cases} \tag{6}$$

The mean runoff rate is therefore

$$\bar{R} = \bar{P}\exp\left(-\frac{I}{\bar{P}}\right). \tag{7}$$

Sediment Transport by Runoff

The instantaneous rate of sediment transport by runoff is modeled as a function of excess shear stress,

$$Q_s = k_f W(\tau - \tau_c)^p, \tag{8}$$

where Q_s is the sediment transport rate integrated across the width of a channel or rill, W is channel width, τ is average bed shear stress, τ_c is critical shear stress for sediment entrainment, k_f is a transport coefficient, and p is an exponent typically on the order of 1.5-3 for bedload (e.g., Yang, 1996) and ~2.5 for suspended load (Whipple et al., 1998). Assuming steady, uniform flow and adopting an empirical bed friction relationship (such as the Manning-Strickler or Darcy-Weisbach relation), shear stress can be expressed as a power function of discharge, Q, and slope, S,

$$\tau = k_t\left(\frac{Q}{W}\right)^{\alpha} S^n, \tag{9}$$

with k_t, α, and n as parameters. (Derivations are given by Willgoose et al., 1991; Howard et al., 1994; Tucker and Slingerland, 1997). Substituting the empirical width-discharge relationship $W = k_w Q^{\omega}$,

$$Q_s = k_f k_w Q^{\omega} (k_t k_w^{-\alpha} Q^m S^n - \tau_c)^p, \tag{10}$$

where $m = \alpha(1-\omega)$.

To write Q in terms of runoff, we use the simple steady-state relationship

$$Q = \int_A R(a)da, \tag{11}$$

where R is runoff per unit area and A is drainage area. If R is uniform across the basin, as we assume in the analysis below, this becomes

$$Q = RA. \tag{12}$$

This is clearly a simplification, first because it neglects variable source-area runoff production, and second because it neglects hydrograph attenuation by equating hydrograph duration with storm duration. The latter effect can in principle be accounted for by relating hydrograph duration and peak attenuation to basin geometric parameters such as total stream length, though for the sake of simplicity we do not do so here.

Sensitivity of Erosion Rate to Rainfall Variability

Fluvial sediment transport can be viewed as a random process in time which in turn is a function of another random process, runoff. We can combine the models derived above for rainfall and sediment transport to analyze the sensitivity of long-term mean sediment transport rate to the

degree of temporal variability in rainfall.

We start by considering only sediment transported during storm events, which for most rivers constitutes the bulk of sediment carried. Under this condition, the mean annual sediment flux is equal to the mean transport rate produced by a storm times the mean storm duration times the number of storms per year, or

$$\langle Q_s \rangle = N \overline{T_r} \overline{Q_s}, \tag{13}$$

where $\langle Q_s \rangle$ is the long-term mean transport rate (mean annual, if $\overline{T_r}$ is in years), N is the average number of storms per year, $\overline{T_r}$ is mean storm duration, and $\overline{Q_s}$ is the mean transport rate produced by a storm.

Note that $\langle Q_s \rangle$ can be related to mean annual rainfall. Mean annual rainfall, $\langle P \rangle$, is equal to mean storm rainfall times storm frequency times mean storm duration,

$$\langle P \rangle = \bar{P} N \overline{T_r}. \tag{14}$$

Combining equations (13) and (14),

$$\langle Q_s \rangle = \frac{\langle P \rangle}{\bar{P}} \overline{Q_s}. \tag{15}$$

The parameter $\bar{P} / \langle P \rangle$, the ratio of mean rainfall intensity to mean annual rainfall, can be thought of as a climate variability factor.

It remains now to determine the mean storm sediment transport rate, $\overline{Q_s}$. We make the following assumptions:

1. Each storm can be approximated as having a constant rainfall rate throughout its duration.
2. At each point in the landscape, runoff (if nonzero) produces a constant, steady discharge equal to the runoff rate times contributing area.
3. Runoff rate per unit area has the exponential distribution given in equation (6).

The steady discharge assumption allows us to write the average storm sediment transport rate as

$$\overline{Q_s} = \int_0^\infty f(R) Q_s(R) dR . \tag{16}$$

Substituting the sediment transport formula (equations (10) and (12)) and the runoff distribution (equation (6)),

$$\overline{Q_s} = \frac{k_f k_w A^\omega}{\bar{P}} \int_0^\infty \exp\left(-\frac{(R+I)}{\bar{P}}\right) R^\omega (k_t k_w^{-\alpha} A^m R^m S^n - \tau_c)^p dR . \tag{17}$$

We do not know of a general analytical solution to this equation, but an analytical solution can be found for the special case τ_c=0, I=0. In that case,

$$\overline{Q_s} = \frac{k_t k_f k_w^{(1-\alpha)} A^\gamma S^{np}}{\bar{P}} \int_0^\infty \exp\left(-\frac{R}{\bar{P}}\right) R^\gamma dR , \tag{18}$$

where $\gamma = mp+\omega$. The integral term can be solved by the substitution $u = R/\bar{P}$, which gives

$$\overline{Q_s} = k_t k_f k_w^{(1-\alpha)} A^\gamma S^{np} \bar{P}^\gamma \int_0^\infty \exp(-u) u^\gamma du = k_t k_f k_w^{(1-\alpha)} A^\gamma S^{np} \bar{P}^\gamma \Gamma(\gamma+1) , \tag{19}$$

where $\Gamma()$ is the gamma function. Combining with equation (15) gives the expected mean annual transport rate:

$$\langle Q_s \rangle = \langle P \rangle \bar{P}^{\gamma-1} k_t k_f k_w^{(1-\alpha)} A^\gamma S^{np} \Gamma(\gamma+1) . \tag{20}$$

Assuming that γ ranges from ~1-2, as is typical, this equation predicts that long-term average sediment transport rates should generally be more sensitive to mean annual rainfall than to mean rainfall intensity, as long as the threshold and infiltration terms are negligible.

Nondimensionalization

To facilitate numerical analysis of equation (19), the equation is nondimensionalized as follows. Rainfall and runoff intensity are normalized by mean annual rainfall, and shear stress and critical shear stress are normalized by the shear stress that would be produced by the mean annual rainfall (at a given slope and contributing area).

Nondimensional rainfall intensity $$P' = P / \langle P \rangle \quad (21)$$

Runoff rate $$R' = R / \langle P \rangle \quad (22)$$

Channel width $$W' = K_w \left(\frac{Q}{Q_p} \right)^{\varpi} \quad (23)$$

Shear stress $$\tau' = \frac{\tau}{\tau_p} = \left(\frac{Q}{Q_p} \right)^{\alpha} \left(\frac{W}{W_p} \right)^{-\alpha} = \left(\frac{Q}{Q_p} \right)^{\alpha} \left(\frac{Q}{Q_p} \right)^{-\alpha\varpi} = R'^{m} \quad (24)$$

Critical shear stress $$\tau_c' = \frac{\tau_c}{\tau_p} \quad (25)$$

Infiltration rate $$I' = \frac{I}{\langle P \rangle} \quad (26)$$

Storm transport rate $$Q_s' = \frac{W(\tau - \tau_c)^p}{W_p \tau_p} = R'^{\varpi} (R'^{m} - \tau_c')^p \quad (27)$$

Mean annual transport rate $$\langle Q_s \rangle' = \frac{1}{\bar{R}'} \exp\left(-\frac{I'}{I' + R'} \right) \overline{Q_s}' \quad (28)$$

Here, W_p refers to $W(<P>)$, and similarly for Q_p and τ_p. Parameter $m=\alpha(1-\omega)$. The nondimen-

sionalization reduces the equation to three dimensionless parameters: I', τ_c', and either P' or R' (in addition to the exponent terms).

Sensitivity to Runoff Variability: Numerical Solutions

In order to analyze the relationship between mean transport rate and the three parameters describing rainfall intensity, infiltration capacity, and critical shear stress, the nondimensional form of equation (17) is solved using a Monte Carlo approach. For each set of parameters $\bar{P}'$, I', and τ_c', 10,000 random values of P' were chosen and the corresponding Q_s' was computed for each. The random Q_s' values were then averaged and multiplied by $1/\bar{P}$ to obtain $\langle Q_s \rangle'$ (see equation (28)). The results are plotted in Figure 1.

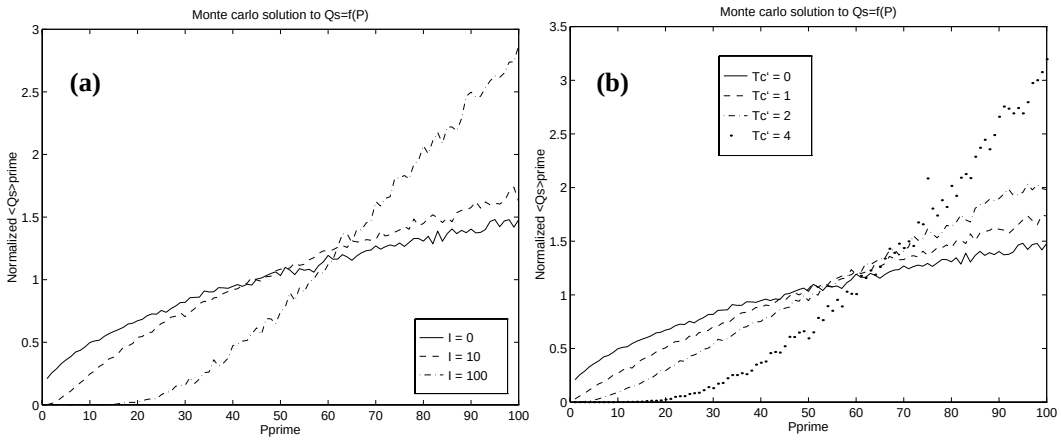

FIGURE 1. Plot of normalized mean sediment flux $\langle Q_s \rangle'$ versus the rainfall variability parameter $\bar{P}'$, showing how the relationship changes as a function of (a) infiltration rate I' and (b) critical shear stress τ_c'. Each plotted point represents an average of 10,000 realizations of Q_s'. To facilitate comparison between the curves, each curve is normalized by the mean value of $\langle Q_s \rangle'$. Exponent parameters are $\varpi = 0.5$, $m = 1/3$, and $p = 3$.

Figure 1a illustrates how the infiltration parameter I' influences the relationship between mean sediment discharge and rainfall variability. With $I'=0$ and $\tau_c'=0$, mean sediment discharge increases as the square root of rainfall intensity, as predicted by equation (20) for $\gamma=\omega+mp=3/2$. By comparison, equation (20) predicts a linear relationship between mean sediment discharge and

mean rainfall, so that for low I' and τ_c', sediment discharge is more sensitive to the total amount of rainfall than to rainfall variability. As I' increases, however, sensitivity to rainfall variability rises as increasingly larger rainfall events are required to produce significant runoff. Which of these curves is most appropriate to natural catchments? A rough estimate can be obtained from published figures. Dunne (1978) reports measurements of infiltration capacity on the order of 0.2 - 6 cm/hr for midwestern agricultural silt-loam soils, and on the order of 8 cm/hr for vegetated forest soils. Given a typical mean annual rainfall of ~1 meter, these values correspond to $I' \sim 20 - 700$, implying that vegetated soils may have the effect of amplifying the importance of rainfall variability. On the other hand, this analysis does not account for direct runoff from saturated areas, which would tend to increase the importance of smaller storms. The analysis also does not account for antecedent soil moisture. In natural catchments, the distribution of interstorm periods influences the likelihood of precipitation falling on already-saturated soils, and is therefore also a potentially important variable.

The relationship between mean sediment discharge and rainfall variability is quite sensitive to the shear stress threshold τ_c', underscoring the point made by Baker (1977) that extreme events become increasingly important in bedrock channels and/or channels bearing very coarse bedload material. Because τ_c' depends on the mean-flow shear stress of the stream in question, it is difficult to judge what typical values might be. An additional complication is the finding by Parker (1978a,b) that channel geometry in streams with mobile bed and banks tends to adjust such that the ratio $\tau/\tau_c \sim K_{ch}$ = constant. Clearly, however, there exists the possibility for high sensitivity to climate variability in the case of boulder-bed or bedrock channels.

Morphologic Consequences of Rainfall Variability: Numerical Example

The consequences of rainfall variability for catchment evolution are next explored through simulations with the CHILD model. Figure 2 shows a synthetic catchment formed by a combination of steady tectonic uplift relative to the outlet at a rate of 2 x 10^{-5} m/yr, and erosion by a sequence of random storm events. In this simulation, mean annual rainfall is 1 meter, mean rainfall intensity is 10 m/yr (~27.4 mm/day), and infiltration capacity I_c = 10 m/yr. The topography consists of a main valley axis flanked by a series of hollows (first-order valleys).

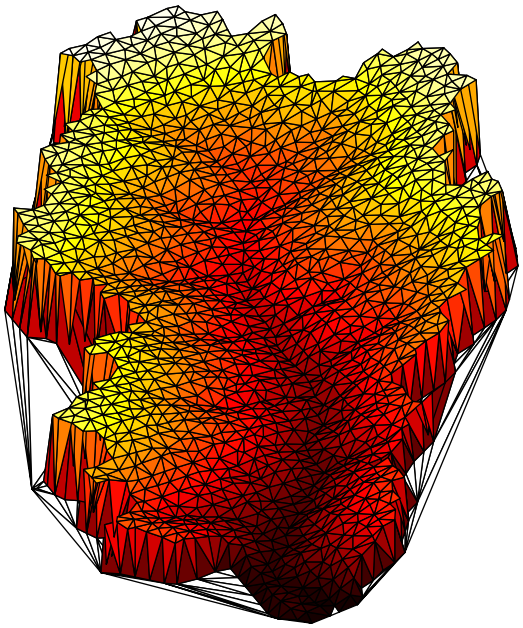

FIGURE 2. Simulated drainage basin formed by a combination of steady tectonic uplift and storms of variable intensity and duration.

Figure 3 illustrates what happens when the catchment in Figure 2 is subjected to a tenfold increase in mean rainfall intensity, with mean annual rainfall held constant, for a total duration of 100,000 model years. The increased efficiency of stream erosion (predicted by equation (20)) leads to accelerated erosion of the channel network (Figure 3b). Erosion is greatest within the first-order valleys, which extend headward to produce a significant increase in drainage density (Figure 3a). When the mean rainfall intensity later reverts to its original value (Figure 4), the pat-

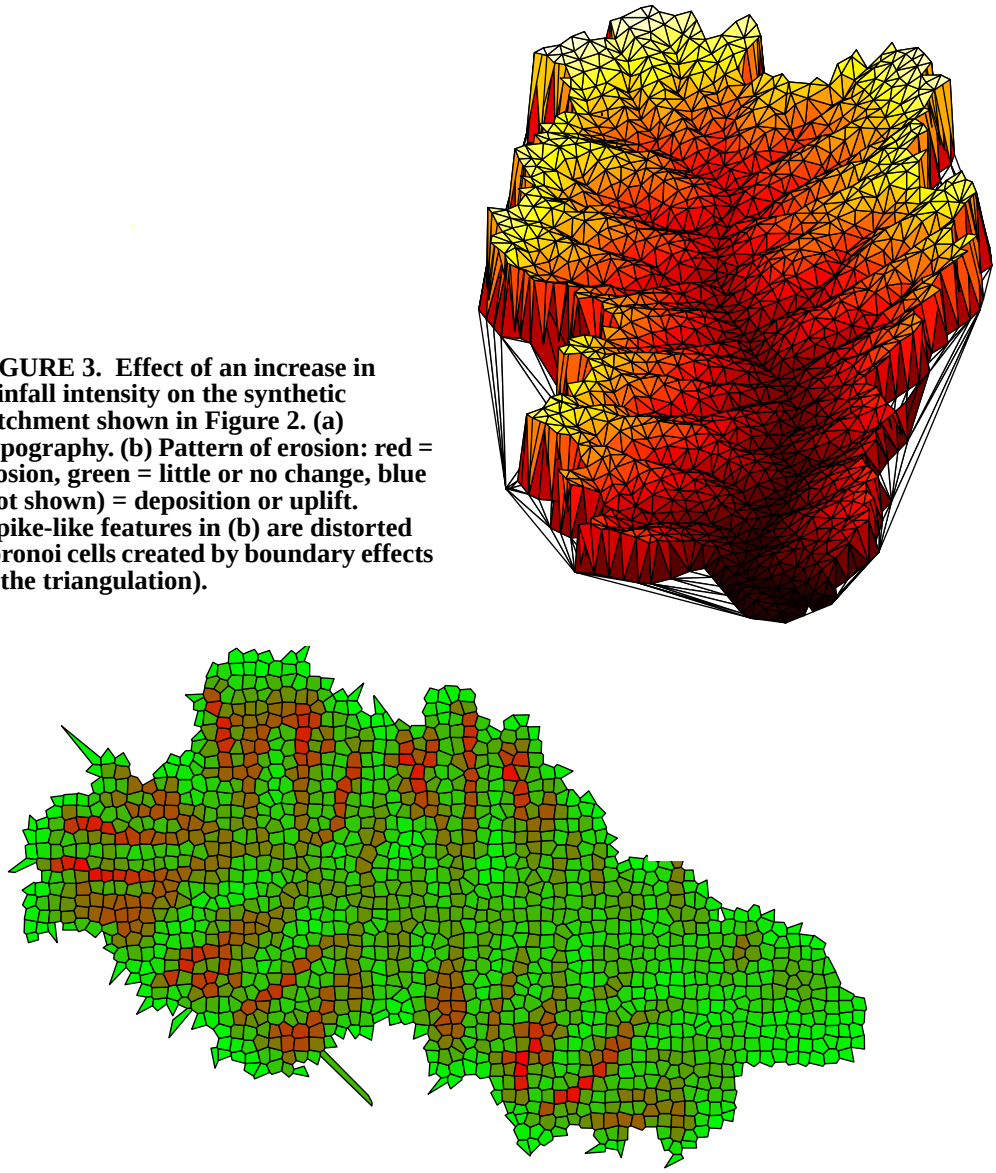

FIGURE 3. Effect of an increase in rainfall intensity on the synthetic catchment shown in Figure 2. (a) Topography. (b) Pattern of erosion: red = erosion, green = little or no change, blue (not shown) = deposition or uplift. (Spike-like features in (b) are distorted Voronoi cells created by boundary effects in the triangulation).

tern reverses as the valley network begins to fill in with sediment.

The morphologic changes illustrated in Figures 2–4 are apparent on a plot of local slope versus contributing area (Figure 5). Initially, the slope-area relationship is close to the equilibrium value predicted by equation (20) (the small difference is due to the fact that the simulation has not yet reached complete equilibrium between uplift and erosion) (Figure 5a). The increase in rainfall intensity (Figure 5b) leads to a decrease in gradient along the main valley network as the catch-

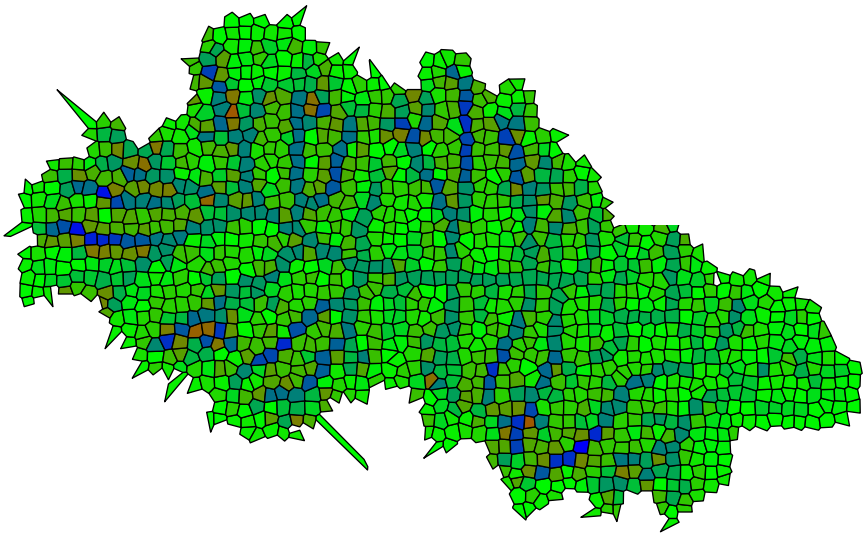

FIGURE 4. Erosion and deposition pattern following a decrease in mean rainfall intensity (to its original value in the simulation show in Figure 2). Initial condition is the topography in Figure 3. Catchment is shown 10,000 model years after decrease in mean rainfall intensity. Blue = net deposition, red = net erosion, and green = little or no change.

ment adjusts toward a new equilibrium (dashed line). At the same time, however, gradients along the first-order valleys and hillslopes increase in response to headward valley erosion and a consequent steepening of side-slopes.

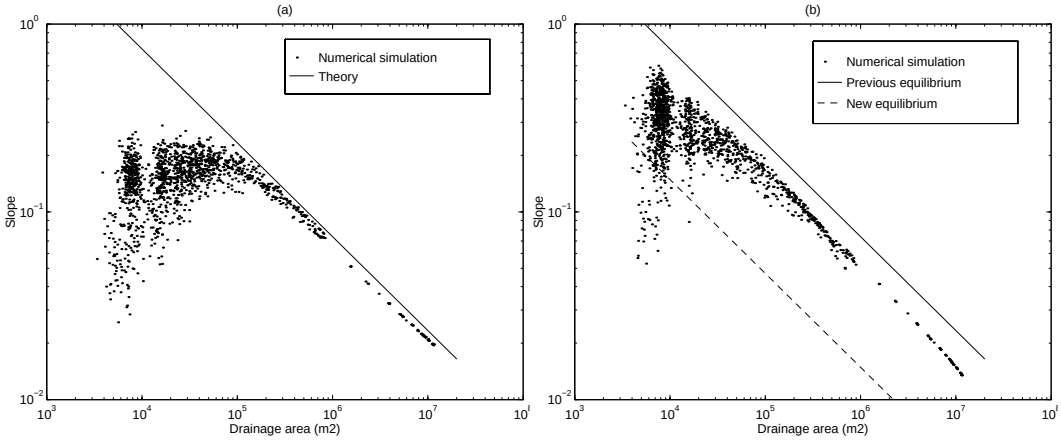

FIGURE 5. Plot of local slope versus contributing area for the numerical simulations shown in (a) Figure 2 and (b) Figure 3. Lines show the equilibrium slope-area relationship calculated by solving equation (20) for slope, under the condition <Qs> = UA (uplift rate times drainage area).

This numerical example illustrates the predicted relationship between rainfall intensity,

catchment relief, and drainage density. One implication of the model is that all else being equal, higher rainfall intensity should be correlated with lower overall relief, higher drainage density, and/or higher sediment flux. The model also implies a pattern valley erosion and valley infilling, respectively, in response to variations in rainfall intensity, though the nature and pattern of response may vary depending on the magnitude of erosion thresholds (Tucker and Slingerland, 1997) and vegetation cover (Section I-E). These predictions thus provide a basis for comparison with morphologic and sediment flux data.

Climatic factors such as mean rainfall and rainfall variability are often closely correlated with vegetation cover, a variable that also can clearly have important geomorphic consequences. In Section I-E, we develop a model for the interaction of vegetation and erosion and use the model to explore some of those consequences.

References

Andrews, E.D., 1980, Effective and bankfull discharges of streams in the Yampa River basin, Colorado and Wyoming: Journal of Hydrology, v. 46, p. 311-330.

Ashmore, P.E., and Day, T.J., 1988, Effective discharge for suspended sediment transport in streams of the Saskatchewan River basin: Water Resources Research, v. 24, no. 6, p. 864-870.

Baker, V.R., 1977, Stream-channel response to floods, with examples from central Texas: Geological Society of America Bulletin, v. 88, p. 1057-1071.

Dunne, T., 1978, Field studies of hillslope flow processes, in Kirkby, M.J., ed., Hillslope Hydrology, New York, John Wiley and Sons, Inc, p. 227-293.

Eagleson, P.S., 1978, Climate, soil, and vegetation: 2. the distribution of annual precipitation derived from observed storm sequences: Water Resources Research, v. 14, p. 713-721.

Harvey, A.M., 1977, Event frequency in sediment production and channel change, in Gregory, K.J., ed., River Channel Change, New York, John Wiley and Sons, Inc.

Howard, A.D., Dietrich, W.E., and Seidl, M.A., 1994, Modeling fluvial erosion on regional to continental scales: Journal of Geophysical Research, v. 99, p. 13,971-13,986.

Parker, 1978a, Self-formed straight rivers with equilibrium banks and mobile bed. Part 1. The sand-silt river: J. Fluid Mech, v. 89, p.109-125

Parker, 1978b, Self-formed straight rivers with equilibrium banks and mobile bed. Part 2. The gravel river: J. Fluid Mech, v. 89, p.127-148.

Tucker, G.E., and Slingerland, R.L., 1997, Drainage basin response to climate change: Water Resources Research, v. 33, no. 8, p. 2031-2047.

Webb, B.W., and Walling, D.E., 1982, The magnitude and frequency characteristics of fluvial transport in a Devon drainage basin and some geomorphological implications: Catena, v. 9, p. 9-23.

Whipple, K.X., Parker, G., Paola, C., and Mohrig, D., 1998, Channel dynamics, sediment transport, and the slope of alluvial fans: experimental study, Journal of Geology, v. 106, p. 677-693.

Willgoose, G.R., Bras, R.L., and Rodriguez-Iturbe, I., 1991, A physically based coupled network growth and hillslope evolution model, 1, theory: Water Resources Research, v. 27, p. 1671-1684.

Wolman, M.G., and Gerson, R., 1978, Relative scales of time and effectiveness in watershed geomorphology: Earth Surface Processes, v. 3, p. 189-208.

Wolman, M.G., and Miller, J.P., 1960, Magnitude and frequency of forces in geomorphic processes: Journal of Geology, v. 68, p. 54-74.

Yang, C.T., 1996, Sediment transport: theory and practice: New York, McGraw Hill, 396pp.